Optimal Environmental Conditions and Anomalous Ecosystem Responses: Constraining Bottom-up Controls of Phytoplankton Biomass in the California Current

Michael G. Jacox*[1,2], Elliott L. Hazen[2], and Steven J. Bograd[2]

[1]Institute of Marine Sciences, University of California, Santa Cruz, CA, USA

[2]Environmental Research Division, Southwest Fisheries Science Center, NOAA, Monterey, CA, USA

*Corresponding Author:

Michael G. Jacox, NOAA/NMFS, Southwest Fisheries Science Center, Environmental Research Division, 99 Pacific Street, Suite 255A, Monterey, CA 93940, USA

(mjacox@ucsc.edu)

Abstract

In Eastern Boundary Current systems, wind-driven upwelling drives nutrient-rich water to the ocean surface, making these regions among the most productive on Earth. Bottom-up regulation of productivity by changing wind and/or nutrient conditions can dramatically impact ecosystem functioning, though the mechanisms are not well understood beyond broad-scale relationships. Here we show the dependence of phytoplankton biomass in nearshore and offshore environments on two key environmental parameters: subsurface nitrate concentration and surface wind stress. In general, moderate wind stress and high nitrate concentrations yield maximal biomass near shore, while offshore biomass is governed primarily by a positive correlation with nitrate concentration. However, due to nonlinear interactions between the influences of wind and nitrate, bottom-up control of primary production cannot be described by either one alone, nor by a combined metric such as nitrate flux. We quantify optimal environmental conditions for phytoplankton, defined as the wind/nitrate space that maximizes chlorophyll concentration, and present a framework for evaluating past and future ecosystem change relative to environmental drivers. The utility of this framework is demonstrated by (i) elucidating anomalous past ecosystem responses in the northeast Pacific, and (ii) providing a mechanistic basis for assessing biological impacts of projected climate change.

Introduction

Eastern Boundary Current ecosystems (EBCs) are highly productive regimes that support rich and diverse biological communities from phytoplankton to top predators[1,2]. Upwelling-driven nitrate flux to the euphotic zone, forced by equatorward alongshore wind, is the foundation for the high biological productivity of these regions[3], and changes in the upwelled nitrate supply have been invoked to explain ecosystem change on seasonal[4] to multi-decadal[5,6] timescales. Such explanations for ecosystem change typically invoke a chain of events whereby increased (decreased) upwelling leads to greater (lower) nitrate supply and subsequently enhanced (reduced) primary productivity, a paradigm that is supported by broad-scale (seasonal, regional) patterns. For example, the annual onset of persistent equatorward wind off California (i.e., the 'spring transition') supplies nitrate to the sunlit surface layer that in turn stimulates substantial new production[7].

However, a growing body of literature suggests the existence of a non-monotonic relationship between alongshore wind and the biological response, in which strong winds limit productivity and phytoplankton biomass through various physical mechanisms. Huntsman and Barber[8] describe the potential for light limitation due to deepening of the surface mixed layer at high wind speeds, and a number of modeling and observational studies cite subduction and/or offshore advection as common mechanisms for removal of nutrients and organic matter from the nearshore euphotic zone during upwelling-favorable conditions[9-16]. Previous studies have found that moderate wind speeds are optimal for nearshore phytoplankton populations[17,18], however they are either idealized or geographically limited, and do not explicitly consider variability in the subsurface nitrate field relative to wind forcing or the interaction between the nearshore and

offshore environments. Furthermore, the supply of nitrate to the surface mixed layer during upwelling can be altered not only by variability in local winds, but also by changes in the water column structure. Remote influences, especially related to basin-scale climate variability (e.g. El Niño-Southern Oscillation, Pacific Decadal Oscillation), can enhance or reduce upwelled nitrate through modification of the nitracline depth as well as the water column stratification and resultant source depth of upwelling[19,20].

In this study, we use a regional ocean model to derive estimates of subsurface nitrate (based on observed temperature-salinity-nitrate relationships) and surface wind stress, and combine them with satellite chlorophyll measurements to explore physical and chemical controls on phytoplankton biomass in the California Current System (CCS). Using data from 1998 to 2010, we define the individual and combined influences of wind and nitrate on chlorophyll concentrations in the nearshore and offshore environments, and use this framework to elucidate the bottom-up forcing behind three periods of highly anomalous ecosystem responses in the CCS: the delayed upwelling season of 2005, anomalous subarctic influence in 2002, and the El Niño/La Niña conditions of 1998-1999. We note at the outset that wind and nitrate are just two contributors to phytoplankton dynamics in the CCS, and many more (e.g., iron, ammonia, zooplankton grazing, others listed in Methods) are not considered here. However, as wind and nitrate are commonly invoked to explain bottom-up ecosystem control, we focus our analysis on them.

Results

Mean environmental conditions

During the upwelling season, a nearshore band extending ~75 km offshore is characterized by mean vertical velocities of several meters per day at the base of the mixed layer, nitrate concentrations of ~5-15 μmol L^{-1} at the base of the mixed layer ($[NO_3]_{MLD}$), and surface chlorophyll concentrations ([chl]) greater than 1 mg m^{-3} (Fig. 1). Surface chlorophyll and $[NO_3]_{MLD}$ in the offshore region (75-300 km from shore) are significantly lower than in the nearshore region but are still higher than concentrations in the oligotrophic subtropical gyre. Vertical velocities in the offshore region are weak and of variable sign, and much of the offshore nutrient and phytoplankton biomass is derived through advection from the nearshore region rather than from local processes[16].

In the alongshore direction, a marked change in the coastal orientation at Cape Mendocino (~40.5˚N) divides the domain into central and northern CCS regions, which experience distinct patterns of atmospheric forcing[21]. The central CCS has generally stronger upwelling and higher $[NO_3]_{MLD}$ than the northern CCS, however [chl] is higher in the northern region (Fig. 1). This discrepancy is especially pronounced north of Cape Blanco and is likely due to regional geographic features including the Strait of Juan de Fuca, the Columbia River, and a relatively wide shelf, all of which facilitate nutrient delivery to the coastal zone[22].

Environmental control of phytoplankton biomass

The dependence of phytoplankton biomass on alongshore wind stress (τ^a) and $[NO_3]_{MLD}$ is shown in Fig. 2 for the nearshore region (0-75 km from shore) and in Fig. 3 for the offshore region (75-300 km). Approximately 1,000 data points (Fig. S1) were used to construct each of the fits shown in Figs. 2 and 3. Data were limited to the upwelling season (March – July for the

central CCS, April – August for the northern CCS), and each data point represents an 8-day mean with an additional 3-point moving average applied, for an effective temporal averaging of 24 days (see Methods for additional details). While the 3-point moving average eliminates some spurious results (e.g., at high wind stress in the nearshore Central CCS), it does not qualitatively change our findings (Fig. S2), suggesting that these relationships hold for time scales of ~1 week – 1 month. Nonetheless, it is important to consider the spatiotemporal averaging of our data when interpreting results, as it may hide important details on shorter time scales (e.g., relaxation events) and finer spatial scales (e.g., retention areas, headlands). Note also that while satellites only observe chlorophyll near the ocean surface, near-surface chlorophyll is highly correlated with depth-integrated chlorophyll off the California coast ($r^2 = 0.9$)[23]. We therefore use [chl] derived from satellite interchangeably with phytoplankton biomass throughout this paper.

While phytoplankton biomass is generally higher in the northern CCS than in the central CCS, its relationship to wind stress and nitrate availability is remarkably similar between the two regions. In the nearshore region, the optimal wind stress for maximal [chl] is ~0.1 N m^{-2} in the central CCS and ~0.1-0.2 N m^{-2} (depending on background nitrate concentration) in the northern CCS (Fig. 2a,d). Chlorophyll is limited when wind stress is weaker or stronger than the optimal value, presumably due to nutrient limitation at low wind stress and physical processes (offshore advection, subduction, mixed layer deepening) at high wind stress. The optimal wind stress of 0.1 N m^{-2} in the central CCS is equivalent to a wind speed of ~8.5 m s^{-1} (ref. 24), falling between optimal wind estimates of ~11.5 m s^{-1} for shelf productivity in a simple model[17], and 5-6 m s^{-1} for pelagic fish recruitment[25]. However, Figs. 2 and 3 also show that identification of an optimal wind intensity tells an incomplete story relative to [chl]. Water column structure, specifically

subsurface nitrate availability, exerts strong control over the biomass attainable at a given wind stress. In the presence of optimal wind stress, [chl] dependence on nitrate is especially strong below $[NO_3]_{MLD} \approx 10$ μmol L^{-1}. In the central CCS for example, when $\tau^a = 0.1$ N m^{-2}, an increase in $[NO_3]_{MLD}$ from 5 to 10 μmol L^{-1} results in ~50% higher [chl] (Fig. 2d).

In the offshore region, [chl] is much less sensitive to alongshore wind stress than it is in the nearshore region (Fig. 3a,d). A weak positive relationship between wind stress and [chl] suggests lateral export of nutrients and/or phytoplankton from the nearshore zone during strong wind events, however reductions in nearshore biomass are not compensated by increases offshore. This finding is consistent with an overall limitation of surface mixed layer productivity in high winds, potentially due to light limitation in a deep mixed layer[8] or to subduction of nutrients and phytoplankton[13]. There is however a clear dependence of offshore [chl] on $[NO_3]_{MLD}$. This relationship may indicate the offshore advection and subsequent uptake of nitrate upwelled near the coast[16]. Similarly, high nitrate in this case may serve as a proxy for iron upwelled from the continental shelf, which can have a critical role in regulating offshore productivity[26]. Alternatively, offshore [chl] may be moderated by wind stress curl driven productivity[27], though there is no significant correlation between [chl] and the magnitude of wind stress curl in the offshore region (r = -0.02 and -0.05 in the northern and central CCS, respectively).

For each [chl] surface fit to τ^a and $[NO_3]_{MLD}$ shown in Figs. 2 and 3, we provide accompanying estimates of scatter around the fit (σ_{data}) and uncertainty in the fit (σ_{fit}). The former is the standard deviation of [chl] data within each pixel of the τ^a -$[NO_3]_{MLD}$ parameter space (see Fig. S1 for scatter plots of all data points), while the latter is the standard deviation of 1,000 fits to the

150 data, each performed with 50% of the data randomly withheld. Data scatter about the fit (σ_{data}) is
151 of the same order of magnitude as the fit itself, indicating substantial unexplained variability due
152 to the many factors outside of wind stress and subsurface nitrate concentration that can influence
153 phytoplankton biomass. Uncertainty in the fits themselves is much smaller, with σ_{fit} typically an
154 order of magnitude smaller than σ_{data}. The lowest values of σ_{fit} occur in data-rich areas of the
155 parameter space, and the diagonal distribution of available data as well as σ_{fit} (especially in Fig.
156 2f) results from a positive correlation between τ^a and $[NO_3]_{MLD}$. Conversely, the largest
157 uncertainties tend to occur in data limited areas of the parameter space, typically at extreme
158 values of τ^a and $[NO_3]_{MLD}$ or where their decoupling is most pronounced. Correlation
159 coefficients for the fits in Figs. 2a, 2d, 3a, and 3e are 0.38, 0.39, 0.49, and 0.47, respectively. The
160 substantial fraction of unexplained variance highlights the influence of other, unaccounted for,
161 variables (detailed in Methods), including some (e.g., temperature, irradiance/day length) that are
162 important particularly on intra-annual timescales. Chlorophyll predictions based on the fits in
163 Figs. 2 and 3 therefore underestimate the observed variance (Fig. S3), and we suggest that they
164 are best used in two ways: (i) to quantify the wind/nitrate space most conducive to high
165 chlorophyll concentrations, and (ii) to predict chlorophyll anomalies when the anomalies are
166 normalized by the interannual variance. The latter is demonstrated in the following sections, in
167 which the relationships of Figs. 2 and 3 are used as a framework for interpreting past events
168 when environmental conditions and phytoplankton responses departed significantly from the
169 climatological state.
170
171 *Delayed upwelling in 2005*

An unusually late shift to upwelling-favorable winds in 2005 had widespread impacts on the northern CCS ecosystem[28], including anomalously warm sea surface temperatures[29], low chlorophyll[30] and zooplankton biomass[31], low mussel and barnacle recruitment[4], and dramatic changes in the populations and distributions of marine nekton[32]. Here we describe the environmental drivers of these effects using the wind stress-nitrate-chlorophyll relationships described by Figs. 2 and 3.

Fig. 4 shows the evolution of $[NO_3]_{MLD}$, τ^a, and [chl] in the northern CCS in a climatological year (Fig. 4a,d) as compared to 2005 (Fig. 4b,e). In a climatological year, winds are poleward in the winter and turn equatorward (upwelling favorable) in March, with peak upwelling occurring in June. Spring upwelling draws deep nitrate-rich water toward the surface, counteracting the influence of solar heating that would otherwise tend to increase stratification, shoal the mixed layer, and inhibit nitrate availability. In 2005, however, alongshore winds remained weak and variable throughout the spring, while the mixed layer shoaled. As a result, $[NO_3]_{MLD}$ fell to concentrations near zero and phytoplankton biomass was anomalously low (Fig. 4c,f). Winds finally turned predominantly equatorward in mid May, marking a spring transition ~1.5 months later than normal. Initially, this shift in winds produced no significant response in [chl], as upwelled waters were nitrate poor. In July, a return of τ^a to near or above climatological values drove a rapid subsequent increase in $[NO_3]_{MLD}$ and stimulated a significant biological response evident in elevated [chl]. The wind-nitrate-chlorophyll relationship shown in Fig. 2a,d predicted the suppression of phytoplankton biomass in spring and early summer as well as a late summer shift to favorable conditions that produced anomalously high biomass (Fig. 4c,f), supporting the paradigm of bottom-up control by wind and nitrate availability.

195

196 Though the seasonal cycle of northern CCS upwelling was highly anomalous in 2005,
197 cumulative wind stress over the entire year was similar to climatological values. The same can be
198 said for mean annual [chl], indicating that while the spring transition was late and the biological
199 response lagged by an additional month or more[33] (Fig. 4), net impacts on primary production
200 were minimal. Similarly, a late season rebound in mussel recruitment off Oregon led to normal
201 overall recruitment in 2005 despite extremely poor recruitment in the early season[4], and nekton
202 generally rebounded by September 2005[32]. However, strong late season recruitment did not
203 compensate for poor early season recruitment of barnacles[4] and zooplankton biomass remained
204 suppressed throughout 2005 and into 2006[31]. The response of higher trophic levels to anomalous
205 environmental conditions is therefore highly varied across species, and in this case is likely
206 influenced by phenological mismatches between predator and prey.
207

208 *Anomalous subarctic influence in 2002*

209 The upwelling season of 2002 was characterized by unusually cold and fresh (i.e., 'minty') waters
210 occupying the upper halocline (30-150 m) off the U.S. west coast, with spiciness anomalies off
211 Oregon equal in magnitude and of opposite sign to those observed during the 1997-1998 El
212 Niño[34]. The proximate cause of these anomalies was wind-driven change in the northeast Pacific
213 circulation; in particular, enhanced southward advection of Subarctic water brought nutrient-rich
214 water and stimulated high primary productivity, especially in the northern CCS (ref. 35 and
215 references therein). As in the previous section, we use the framework of Figs. 2 and 3 to examine
216 anomalous phytoplankton concentrations in the context of environmental drivers.
217

The progressions of τ^a, $[NO_3]_{MLD}$, and [chl] anomalies during 2002 are shown in Fig. 5. Elevated nitrate concentrations arrived in January, reaching levels ~50% higher than normal in the spring, and persisted throughout much of the year. Upwelling favorable winds were also slightly stronger than normal in the spring and late summer, though wind anomalies were much less pronounced than those in the nitrate field. The combination of moderate winds and high nitrate proved ideal for phytoplankton, supporting very high spring and late summer biomass in both the nearshore and offshore environments. Our analysis accurately predicted observed patterns in chlorophyll variability (Fig. 5c,f), though underestimation of positive nearshore [chl] anomalies suggests that we overestimate the pernicious influence of low wind stress (<0.1 N m^{-2}) in the presence of high nitrate concentrations (Fig. 5b,c).

The conditions of 2002 highlight the importance of understanding both local and remote influences when studying biological responses to the environment. In contrast to 2005, when anomalies in the nutrient field were tied to local winds, 2002 brought positive nitrate anomalies to the northern CCS through lateral advection of subarctic water. Because high nitrate concentrations were available immediately beneath the mixed layer, moderately strong local upwelling was able to efficiently supply the surface mixed layer with nutrients, stimulating considerable primary production. This modulation of local productivity by advective processes underscores the strength of considering atmospheric forcing and source water properties together when assessing their impacts on the ecosystem.

El Niño/La Niña events of 1998-1999

240 The 1997-1998 El Niño was by some metrics the strongest on record[36], and was followed by a
241 multi-year La Niña event that signaled a regime shift in the north Pacific climate[37,38]. Ecosystem
242 impacts in the CCS from physics to top predators are well documented (see special issue of
243 Progress in Oceanography, Volume 54, 2002). Again, we place the temporal evolution of the
244 physical and biogeochemical environment in the context of bottom-up controls detailed in the
245 present study.
246
247 Environmental conditions in 1998 and 1999 and their relations to nearshore and offshore
248 chlorophyll concentrations are shown in Fig. 6. El Niño was near peak strength in January 1998,
249 and communication of tropical anomalies through oceanic propagation and atmospheric
250 teleconnection drove strong poleward winds and extremely low $[NO_3]_{MLD}$ in the CCS[39]. Spring
251 and early summer winds were also weaker than normal (Fig. 6a,b), but actually of optimal
252 magnitude to produce high [chl] in the nearshore region given adequate nitrate in the subsurface.
253 However, remote forcing of a deep nitracline by equatorial and coastal wave propagation from
254 the tropics produced an exceptionally deep nitracline and therefore low $[NO_3]$ in upwelling
255 source waters. This effect was exacerbated by anomalously weak local winds and a relatively
256 shallow source depth for upwelling[39], resulting in upwelling season $[NO_3]_{MLD}$ values of ~3-7
257 μmol L^{-1}, well below climatological values of ~10-15 μmol L^{-1} (Fig. 6a,b). Observed
258 phytoplankton biomass was suppressed in both the nearshore and offshore regions, as predicted
259 based on the influences of wind and subsurface nitrate (Fig. 6c,i).
260
261 The switch from El Niño conditions in 1997-1998 to La Niña conditions in 1998-1999 is
262 typically regarded as a return to high productivity. However, while [chl] was uniformly low in

1998, anomalies in 1999 were spatially varied in the cross-shore direction. Early in 1999, $[NO_3]_{MLD}$ was much higher than at the same time in 1998, again consistent with nitracline depth anomalies driven by anomalous atmospheric and basin-scale oceanic forcing during El Niño and La Niña. Similarly, alongshore winds strengthened considerably in 1999, especially in May when τ^a reached levels ~60% higher than climatological values (Fig. 6a,e). Thus, the combination of remote and local influences produced a shallow nitracline and a deep source for upwelling, and $[NO_3]_{MLD}$ climbed as high as 20 μmol L^{-1} in May (~50% higher than the climatological concentration), providing ample nitrate supply to the surface mixed layer. However, such strong wind also drove rapid offshore advection and intense mixing, and Fig. 6e,f suggests that despite elevated nitrate levels, nearshore [chl] in spring/summer was limited by excessive wind stress. Conversely, the conditions of 1999 were optimal for the development of high [chl] offshore, which benefitted from high nitrate concentrations (Fig. 6k,l). Observations from the central CCS in the spring/summer of 1999 support this paradigm; new production anomalies were negative nearshore and positive offshore[40], elevated chlorophyll extended unusually far offshore[41], and reductions or offshore displacements of zooplankton and juvenile fish were attributed to rapid offshore advection driven by strong upwelling[42,43]. Predictions based solely on wind and subsurface nitrate capture the anomalously high [chl] offshore (Fig. 6l) and lower anomalies nearshore, though the adverse effects of high winds appear to be underpredicted for April-June (Fig. 6f).

Interestingly, nearshore [chl] was similarly limited in 1998 and 1999, though by completely different mechanisms (Fig. 6d). In 1998, τ^a was anomalously weak, there was a deep nitracline associated with remote forcing from the tropical El Niño, and resultant low $[NO_3]_{MLD}$ values are

implicated in [chl] limitation. In 1999, $[NO_3]_{MLD}$ was exceptionally high but nearshore [chl] in the spring and early summer was limited by strong winds. Substantial differences in overall system biomass between the two years were therefore driven almost entirely by anomalies of opposite sign in the offshore environment (Fig. 6j), which may be influenced by local curl-driven upwelling or by offshore advection of nearshore nutrients and phytoplankton.

Discussion

In this paper, we present a framework for evaluating bottom-up influences on ecosystem functioning in an Eastern Boundary Upwelling System. We find moderate wind stress to be optimal for accumulation of phytoplankton biomass in the nearshore environment and in the CCS as a whole. Productivity is nutrient limited below the optimal wind stress, while at higher wind stress physical processes (offshore advection, subduction, enhanced mixing) conspire to export nutrients and organic matter either offshore or below the euphotic zone. Conversely, the offshore region appears relatively unaffected by both nearshore wind stress and offshore wind stress curl. In both the nearshore and offshore environments, [chl] correlates positively with subsurface nitrate concentration. These patterns are robust across the dynamically different central and northern CCS regions and constitute our primary result: the isolation of a fundamental relationship between wind, subsurface nitrate, and chlorophyll that emerges amidst many confounding influences (see Methods).

While phytoplankton biomass exhibits relationships with both physical (wind stress) and chemical (nitrate) forcings individually, a key result of our study is that the two have strong interactions in terms of their influences over [chl]. First, nitrate concentration at the base of the

309 mixed layer is dependent on the wind history and its modification of the water column, as well as
310 remotely forced changes in the subsurface nitrate field. The utility of instantaneous wind stress
311 alone as an indicator of potential productivity is therefore limited, even though stronger winds
312 generally correlate to higher nitrate concentrations. Explicit representation of subsurface nitrate
313 in our study negates the need for proxies such as cumulative wind stress and implicitly accounts
314 for changes deeper in the water column structure associated with basin scale climate variability
315 and lateral advection. We are therefore able to explain anomalous events that are driven largely
316 by remote forcing (e.g., the deep nitracline in 1998, anaomlous equatorward advection of
317 subarctic waters in 2002) or by local forcing (e.g., weak/delayed winds in 2005). Second, a lag
318 on the order of a week to a month often exists between a change in alongshore winds (e.g., the
319 start of the upwelling season) and a measurable biological response. Our results suggest that this
320 lag lies primarily in the response of the nutrient field to wind forcing (e.g., Fig. 4b), and that the
321 phytoplankton response is fast (<1 week) once both the wind and nutrient conditions are right.
322 Third, in terms of altering surface chlorophyll concentrations, the impact of changes in either
323 winds or nitrate is dependent on the state of the other. For example, reducing wind stress in the
324 central CCS from 0.2 to 0.1 N m^{-2} would on average produce a ~50% increase in nearshore [chl]
325 when $[NO_3]_{MLD} \approx 15$ μmol L^{-1}, but the same reduction in wind stress would produce no
326 discernible change in [chl] when $[NO_3]_{MLD} \approx 5$ μmol L^{-1} (Fig. 2d). Fourth, a single metric that
327 combines subsurface nitrate and vertical transport (i.e., vertical nitrate flux) is inadequate for
328 characterizing bottom-up control of phytoplankton. For example, weak upwelling of nitrate-rich
329 water and strong upwelling of nitrate-poor water may produce the same vertical nitrate flux.
330 However, the biological response is very different, with the latter characterized by a deep mixed
331 layer, rapid offshore advection, and suppressed phytoplankton biomass. For all of these reasons,

understanding the state of both the winds and the subsurface nitrate field is critical to understanding bottom-up impacts on ecosystem productivity. The examples of 2005, 2002, and 1998-1999 are cases where the biological response to environmental conditions cannot be interpreted based on either wind or nutrient data alone. Similar effects on phytoplankton biomass can result from several distinct mechanisms; for example, we have shown cases where anomalously low nearshore [chl] was driven by a deep nitracline (1998), unusually strong winds (1999), and an interaction whereby anomalously weak equatorward winds caused a drop in subsurface nitrate (2005).

Finally, our results can be used to contextualize ecosystem responses to future changes in coastal upwelling systems. Bakun[44] proposed a mechanism for increased upwelling-favorable winds in a warming world and while the existence of such a trend and its governing dynamics have fueled much debate in recent years, the most recent retrospective analyses and model forecasts suggest that the sign and magnitude of long-term trends in upwelling winds are likely latitude and region dependent[45,46,47]. Our results suggest that intensification of peak upwelling season winds would make them stronger than the optimal value for primary producers in the nearshore environment (Figs. 4a,5a). However, such an increase should also enhance nutrient delivery to the surface mixed layer[20], increasing biomass in the offshore region and at least partially offsetting the negative impact of strong winds on the nearshore region. A wind intensification scenario would also produce optimal wind stress earlier in the year, resulting in an earlier onset and longer duration of the high productivity season. In the case of weakened alongshore winds, summertime productivity in the central CCS could actually be enhanced, provided subsurface nitrate remains near climatological concentrations (Fig. 5a). Alternatively, a dramatic increase in the nitrate

concentration of upwelling source waters (e.g., a doubling by 2100)[48] would likely negate any impact of changes in the winds and result in a highly productive environment (Figs. 2,3). Ultimately, ecosystem impacts arising from each of these scenarios will differ greatly as individual species suffer or prosper based on their sensitivities to the overall magnitude of primary productivity, its phenology, and its spatial distribution.

Methods

Study Domain

Our study domain spans the west coast of the US from Point Conception in the south to southern Washington State in the north (34.5-46.5˚N). As in previous studies (e.g., ref 21), we split this region at Cape Mendocino (40.5˚N) into central CCS and northern CCS domains. In the cross-shore direction we define a nearshore region (0-75 km from shore) characterized in the upwelling season by strong vertical velocities and surface chlorophyll concentrations greater than 1 mg m^{-3} (Fig. 1), and an offshore region (75-300 km from shore) roughly corresponding to the California Current transition zone[26]. Our analysis spans the years 1998-2010, the period of SeaWiFS data availability. As the focus of the study is chlorophyll dependence on wind stress and nitrate concentration, we focus on the upwelling season (March-July for the central CCS, April-August for the northern CCS), when physical transport and nutrient supply are expected to be dominant regulators of primary production. Outside of the upwelling season other processes are likely more important; light limitation in winter months may limit chlorophyll even in the presence of optimal wind and nutrient conditions[14], while in the fall the phytoplankton assemblage is dominated by picoplankton[49] and vertically migrating dinoflagellates[50], which thrive in warm, stratified conditions and are not dependent on upwelling.

Chlorophyll Data

Satellite chlorophyll estimates are from the Sea-viewing Wide Field-of-view Sensor (SeaWiFS) with the NASA/GSFC OC4v4 algorithm[51]. Global daily composite fields, with spatial resolution of 1/12˚, were downloaded from NOAA CoastWatch.

Ocean Model

Wind stress, temperature, salinity, and mixed layer depth were obtained from a historical analysis of the CCS that uses the Regional Ocean Modeling System (ROMS) with 4-Dimensional variational (4D-Var) data assimilation. The analysis spans 1980-2010 and is described in detail elsewhere[52,53]. Surface radiative and freshwater fluxes were derived from the European Centre for Medium-Range Weather Forecasting (ECMWF) 40-year reanalysis (ERA-40)[54] prior to 2002 and from ERA-Interim[55] for 2002-2010. Lateral boundary conditions were taken from the Simple Ocean Data Assimilation (SODA) reanalysis[56]. For the period of this study (1998-2010), wind forcing was derived from the Cross Calibrated Multi Platform (CCMP) product[57]. Data assimilation was performed in 8-day cycles. In each cycle the initial conditions, boundary conditions, and surface forcing were adjusted by the 4D-Var system to improve model representation of observed dynamics[58,59,60]. Assimilated data includes available satellite Sea Surface Temperature (AVHRR, AMSR-E, and MODIS Terra) and Sea Surface Height (AVISO) as well as in situ salinity and temperature measurements from the ENSEMBLES (EN3) database.

Nitrate Model

Nitrate concentration at the base of the mixed layer was calculated as follows: First, available data from the World Ocean Database and the Global Ocean Ecosystem Dynamics (GLOBEC) were used to fit nitrate as a function of temperature and salinity using the Matlab® function gridfit (http://www.mathworks.com/matlabcentral/fileexchange/8998) with a smoothness parameter of 1.5 and 20 nodes in the x and y directions. Temperature-salinity-nitrate fits were constructed separately for the central and northern regions using only data from the upwelling season in order to minimize latitudinal and seasonal biases[62]. Data were further limited to the upper 200 m of the water column and the years of our study (1998-2010). In all, 1049 measurements in the central CCS and 3772 measurements in the northern CCS were used to construct the nitrate relationships, which capture 97% and 91% of the observed variance, respectively (Fig. S4). Next, mixed layer depth in the model was estimated from the temperature and salinity fields according to Kara et al.[61]. Model temperature and salinity at the base of the mixed layer, along with the nitrate fits in Fig. S4, were then used to estimate nitrate concentration at the base of the mixed layer. Validation of our model-based nitrate estimates, using independent training and validation datasets, is shown in Fig. S5. The model-based estimates capture 76% of the observed variance in subsurface nitrate concentration. Note that this validation accounts for uncertainty in both the model representation of subsurface physical properties and the relationship of those properties to subsurface nitrate concentration.

Determining chlorophyll dependence on wind stress and nitrate

Surface chlorophyll concentration ([chl]) was fit as a function of alongshore wind stress (τ^a) and nitrate concentration at the base of the mixed layer ($[NO_3]_{MLD}$. This process is outlined below for one example region (offshore in the northern CCS, i.e., Fig. 3a). These steps were repeated to

423 define the wind stress-nitrate-chlorophyll relationship for each of the four regions in Figs. 2 and
424 3 (nearshore/offshore and northern/central CCS).
425 1. Each variable (τ^a, $[NO_3]_{MLD}$, and [chl]) was averaged over 8-day cycles coincident with
426 the assimilation cycles of the ROMS reanalysis. The 8-day averaging period is consistent
427 with typical timescales for upwelling events (~3-10 days[63]), and for phytoplankton
428 response to an injection of upwelled nutrients (~3-7 days[64]). A three-point moving
429 average was then applied to the 8-day averages, increasing the effective temporal
430 averaging to 24 days.
431 2. The region of interest (for example, offshore in the northern CCS) was further divided
432 into 1˚ latitude bins. Within each bin, τ^a was calculated 75 km from shore and $[NO_3]_{MLD}$
433 was averaged from the coast to 75 km from shore, in order to capture the coastal
434 upwelling influence (Fig. 1). Chlorophyll was averaged over the cross-shore domain of
435 interest (for example, 75-300 km from shore) only if spatial coverage of chlorophyll data
436 was greater than 90%. When chlorophyll coverage is lower, spatial averages become less
437 reliable, particularly with respect to biases in the nearshore region (Fig. S6). We used
438 averages in 1˚ bins instead of the full 6˚ region to maximize the number of points with
439 adequate chlorophyll coverage. Variability among 1˚ bins also allows for more complete
440 coverage of the parameter space when fitting [chl] to τ^a and $[NO_3]_{MLD}$. Note that while
441 [chl] was averaged two different cross-shore regions, τ^a was always calculated 75 km
442 from shore and $[NO_3]_{MLD}$ was always averaged from the coast to 75 km offshore. This
443 approach allows us to determine the distinct nearshore and offshore chlorophyll
444 responses to nitrate supplied by coastal upwelling (e.g., intense coastal upwelling may

445 generate rapid offshore advection of upwelled nutrients and therefore high chlorophyll
446 offshore but not nearshore).
447 3. Using data points generated from steps 1 and 2 (shown as scatter plots in Fig. S1), we fit
448 a [chl] surface to τ^a and $[NO_3]_{MLD}$ using the Matlab® function gridfit
449 (http://www.mathworks.com/matlabcentral/fileexchange/8998) with a smoothness
450 parameter of 1.5 and 20 nodes in the x and y directions.
451
452 *Uncertainty estimates*
453 We include with each surface fit in Figs. 2 and 3 an estimate of variability in the data around the
454 fit, as well as uncertainty in the fit itself. The former is calculated simply as the standard
455 deviation of data points within each pixel, and is labeled as σ_{data}. The latter is estimated with a
456 bootstrap approach in which we fit the data 1000 times, each with 50% of the data randomly
457 withheld. The standard deviation of the 1000 fits provides an estimate of uncertainty in the fit,
458 and is labeled σ_{fit}.
459
460 *Caveats*
461 As detailed above, the [chl] fits to τ^a and $[NO_3]_{MLD}$, which form the basis of our analysis, capture
462 only a moderate portion of the variance in [chl] ($r = 0.38$-0.49). There are many potential
463 contributors to the unexplained variance, including influences of nutrients other than nitrate (e.g.,
464 iron, ammonium), zooplankton grazing, variable light levels and day length within the upwelling
465 season, temporal and spatial autocorrelation of [chl], riverine influences on chlorophyll or on
466 satellite estimates of chlorophyll, decoupling of surface and depth integrated chlorophyll, and
467 uncertainty in our estimates of wind, nitrate, and surface chlorophyll. Given all of these

468 confounding factors, the strength of our analysis is that we are able to extract robust fundamental
469 relationships between wind, nitrate, and chlorophyll. The remarkable qualitative similarity of
470 these relationships between the central and northern CCS speaks to their robustness, as many of
471 the confounding processes listed above vary widely between the two regions.
472
473 *Chlorophyll predictions*
474 Chlorophyll predictions (Figs. 4-6) were made by interpolating modeled τ^a and $[NO_3]_{MLD}$ values
475 onto the fits in Figs. 2a,d and 3a,d. These predictions were made on the same spatiotemporal
476 scales as were used for the fits (i.e., 8-day means with additional 3-point smoothing, 1˚ latitude
477 bins), and were subsequently averaged over the appropriate temporal (monthly) and spatial (e.g.,
478 northern CCS, nearshore) scales. Finally, chlorophyll anomalies for each month were normalized
479 by the standard deviation of predicted chlorophyll across all years. Observed chlorophyll values
480 were similarly averaged monthly and over the desired spatial domain and normalized by the
481 standard deviation of observed chlorophyll values across all years.
482
483 **References**
484 1. Pauly, D. & Christensen, V. Primary production required to sustain global fisheries. *Nature*
485 **374**, 255-257 (1995)
486 2. Block, B. A. et al. Tracking apex marine predator movements in a dynamic ocean. *Nature*
487 **475**, 86-90 (2011).
488 3. Dugdale, R. C. & Goering, J. J. Uptake of new and regenerated forms of nitrogen in primary
489 productivity, *Limnol. Oceanogr.* **12**, 196-206 (1967).
490 4. Barth, J. A. et al. Delayed upwelling alters nearshore coastal ocean ecosystems in the

491 northern California current. *Proc. Nat. Acad. Sci.* **104**, 3719-3724 (2007).
492 5. Roemmich, D. & McGowan, J. Climatic warming and the decline of zooplankton in the
493 California Current. *Science* **267**, 1324-1326 (1995).
494 6. Chavez, F. P., Ryan, J., Lluch-Cota, S. E. & Ñiquen, M. From anchovies to sardines and
495 back: multidecadal change in the Pacific Ocean. *Science* **299**, 217-221 (2003).
496 7. Lynn, R. J., Bograd, S. J., Chereskin, T. K., Huyer, A. Seasonal renewal of the California
497 Current: The spring transition off California. *J. Geophys. Res.* **108** (2003).
498 8. Huntsman, S. A. & Barber, R. T. Primary production off northwest Africa: the relationship to
499 wind and nutrient conditions. *Deep Sea Research* **24**, 25-33 (1977).
500 9. Barth, J. A. et al. Injection of carbon from the shelf to offshore beneath the euphotic zone in
501 the California Current. *J. Geophys. Res.* **107** (2002).
502 10. Bograd, S. J. & Mantyla, A. W. On the subduction of upwelled waters in the California
503 Current. *J. Mar. Res.* **63**, 863-885 (2005).
504 11. Plattner, G. K., Gruber, N., Frenzel, H. & McWilliams, J. C. Decoupling marine export
505 production from new production. *Geophys. Res. Lett.* **32** (2005).
506 12. Lathuilière, C., Echevin, V., Lévy, M., & Madec, G. On the role of the mesoscale circulation
507 on an idealized coastal upwelling ecosystem. *J. Geophys. Res.* **115** (2010).
508 13. Gruber, N. et al. Eddy-induced reduction of biological production in eastern boundary
509 upwelling systems. *Nature Geoscience* **4**, 787-792 (2011).
510 14. Messié, M. & Chavez, F. P. Seasonal regulation of primary production in eastern boundary
511 upwelling systems. *Prog. Oceanogr.* **134**, 1-18 (2015).
512 15. Evans, W., Hales, B., Strutton, P. G., Shearman, R. K. & Barth, J. A. Failure to bloom:
513 Intense upwelling results in negligible phytoplankton response and prolonged CO2

514 outgassing over the Oregon shelf. *J. Geophys. Res.* **120**, 1446-1461 (2015).
515 16. Nagai, T. et al. Dominant role of eddies and filaments in the offshore transport of carbon and
516 nutrients in the California Current System. *J. Geophys. Res.* (2015).
517 17. Botsford, L. W., Lawrence, C. A., Dever, E. P., Hastings, A. & Largier, J. Wind strength and
518 biological productivity in upwelling systems: an idealized study. *Fish. Oceanogr.* **12**, 245-
519 259 (2003).
520 18. García-Reyes, M., Largier, J. L. & Sydeman, W. J. Synoptic-scale upwelling indices and
521 predictions of phyto- and zooplankton populations. *Prog. Oceanogr.* **120**, 177-188 (2014).
522 19. Chhak, K., & Di Lorenzo, E. Decadal variations in the California Current upwelling cells.
523 *Geophys. Res. Lett.* **34** (2007).
524 20. Jacox, M. G., Bograd, S. J., Hazen, E. L. & Fiechter, J. Sensitivity of the California Current
525 nutrient supply to wind, heat, and remote ocean forcing. *Geophys. Res. Lett*. **42** (2015).
526 21. Dorman, C. E. & Winant, C. D. Buoy observations of the atmosphere along the west coast of
527 the United States, 1981–1990. *J. Geophys. Res.* **100**, 16029-16044 (1995).
528 22. Hickey, B. M. & Banas, N. S. Why is the northern end of the California Current System so
529 productive? *Oceanography* **21**, 90-107 (2008).
530 23. Frolov, S., Ryan, J. P. & Chavez, F. P. Predicting euphotic‐depth‐integrated chlorophyll‐a
531 from discrete‐depth and satellite‐observable chlorophyll‐a off central California. *J. Geophys.*
532 *Res.* **117** (2012).
533 24. Large, W. & Pond, S. Open Ocean momentum flux measurements in moderate to strong
534 winds. *J. Phys. Oceanogr.,* **11**, 324-336 (1981).
535 25. Cury, P. & Roy, C. Optimal environmental window and pelagic fish recruitment success in
536 upwelling areas. *Can. J. Fish. Aquat. Sci.* **46**, 670-680 (1989).

537 26. Biller, D. V. & Bruland, K. W. The central California Current transition zone: a broad region
538 exhibiting evidence for iron limitation. *Prog. Oceanogr.* **120**, 370-382 (2014).
539 27. Rykaczewski, R. R. & Checkley, D. M. Influence of ocean winds on the pelagic ecosystem in
540 upwelling regions. *Proc. Nat. Acad. Sci.* **105**, 1965-1970 (2008).
541 28. Schwing, F. B.et al. Delayed coastal upwelling along the US West Coast in 2005: A
542 historical perspective. *Geophys. Res. Lett.* **33** (2006).
543 29. Pierce, S. D., Barth, J. A., Thomas, R. E. & Fleischer, G. W. Anomalously warm July 2005
544 in the northern California Current: Historical context and the significance of cumulative wind
545 stress. *Geophys. Res. Lett.* **33** (2006).
546 30. Thomas, A. C. & Brickley, P. Satellite measurements of chlorophyll distribution during
547 spring 2005 in the California Current. *Geophys. Res. Lett.* **33** (2006).
548 31. Mackas, D. L., Peterson, W. T., Ohman, M. D. & Lavaniegos, B. E. Zooplankton anomalies
549 in the California Current system before and during the warm ocean conditions of 2005.
550 *Geophys. Res. Lett.* **33** (2006).
551 32. Brodeur, R. D. et al. Anomalous pelagic nekton abundance, distribution, and apparent
552 recruitment in the northern California Current in 2004 and 2005. *Geophys. Res. Lett.* **33**
553 (2006).
554 33. Kosro, P. M., Peterson, W. T., Hickey, B. M., Shearman, R. K. & Pierce, S. D. Physical
555 versus biological spring transition: 2005. *Geophys. Res. Lett.* **33** (2006).
556 34. Freeland, H. J., Gatien, G., Huyer, A. & Smith, R. L. Cold halocline in the northern
557 California Current: An invasion of subarctic water. *Geophys. Res. Lett.*, **30** (2003).
558 35. Huyer, A. Preface to special section on enhanced Subarctic influence in the California
559 Current, 2002. *Geophys. Res. Lett.*, **30** (2003).

560 36. McPhaden, M. J. Genesis and evolution of the 1997-98 El Niño. *Science* **283**, 950-954
561 (1999).
562 37. Peterson, W. T. & Schwing, F. B. A new climate regime in northeast Pacific ecosystems.
563 *Geophys. Res. Lett.* **30** (2003).
564 38. England, M. H. et al. Recent intensification of wind-driven circulation in the Pacific and the
565 ongoing warming hiatus. *Nature Climate Change* **4**, 222-227 (2014),
566 39. Jacox, M. G., Fiechter, J., Moore, A. M. & Edwards, C. A. ENSO and the California Current
567 coastal upwelling response. *J. Geophys. Res.* **120**, 1691-1702 (2015).
568 40. Kudela, R. M. & Chavez, F. P. Multi-platform remote sensing of new production in central
569 California during the 1997–1998 El Nino. *Prog. Oceanogr.* **54**, 233-249 (2002).
570 41. Bograd, S. J. et al. The state of the California Current, 1999-2000: Forward to a new regime?
571 *Rep. Calif. Coop. Ocean. Fish. Invest.* **41**, 26-52 (2000).
572 42. Hopcroft, R. R., Clarke, C. & Chavez, F. P. Copepod communities in Monterey bay during
573 the 1997–1999 El Niño and La Niña. *Prog. Oceanogr.* **54**, 251-264 (2002).
574 43. Schwing, F. B., Moore, C. S., Ralston, S. T. & Sakuma, K. M. Record coastal upwelling in
575 the California Current in 1999. *Rep. Calif. Coop. Ocean. Fish. Invest.* **41**, 148-160 (2000).
576 44. Bakun, A. Global climate change and intensification of coastal ocean upwelling. *Science* **247**,
577 198-201 (1990).
578 45. Sydeman, W. J. et al. Climate change and wind intensification in coastal upwelling
579 ecosystems. *Science* **345**, 77-80 (2014).
580 46. Rykaczewski, R. R. et al. Poleward displacement of coastal upwelling-favorable winds in the
581 ocean's eastern boundary currents through the 21st century. *Geophys. Res. Lett*. (2015).
582 47. Wang, D., Gouhier, T. C., Menge, B. A. & Ganguly, A. R. Intensification and spatial

583 homogenization of coastal upwelling under climate change, *Nature* **518**, 390-394 (2015).
584 48. Rykaczewski, R. R. & Dunne, J. P. Enhanced nutrient supply to the California Current
585 Ecosystem with global warming and increased stratification in an earth system model.
586 *Geophys. Res. Lett.* **37** (2010).
587 49. Pennington, J. T. & Chavez, F. P. Seasonal fluctuations of temperature, salinity, nitrate,
588 chlorophyll and primary production at station H3/M1 over 1989–1996 in Monterey Bay,
589 California. *Deep Sea Res. Part II* **47**, 947-973 (2000).
590 50. Ryan, J. P. et al. Influences of upwelling and downwelling winds on red tide bloom dynamics
591 in Monterey Bay, California. *Cont. Shelf Res.* **29**, 785-795 (2009).
592 51. O'Reilly, J.E. et al. Ocean color chlorophyll algorithms for SeaWiFS. *J. Geophys. Res.* **103**,
593 937-953 (1998).
594 52. Neveu, E. et al. An historical analysis of the California Current circulation using ROMS 4D-
595 Var. Part I: System configuration and diagnostics. *Ocean Modelling* (2015).
596 53. Jacox, M. G., Moore, A. M., Edwards, C. A. & Fiechter, J. Spatially resolved upwelling in
597 the California Current System and its connections to climate variability. *Geophys. Res. Lett.*
598 **41**, 3189-3196 (2014).
599 54. Uppala, S. M. et al. The ERA‐40 re‐analysis. *Q. J. R. Meteorol. Soc.* **131**, 2961-3012 (2005).
600 55. Dee, D. P. et al. (2011), The ERA-Interim reanalysis: configuration and performance of the
601 data assimilation system, *Q.J.R. Meteorol. Soc.* **137**, 553-597.
602 56. Carton, J. A. & Giese, B. S. A reanalysis of ocean climate using Simple Ocean Data
603 Assimilation (SODA). *Mon. Weath. Rev.* **136**, 2999-3017 (2008).
604 57. Atlas, R. et al. A cross-calibrated, multiplatform ocean surface wind velocity product for
605 meteorological and oceanographic applications. *Bull. Am. Meteorol. Soc.* **92**, 157–174

606 (2011).
607 58. Moore, A. M. et al. The Regional Ocean Modeling System (ROMS) 4-dimensional
608 variational data assimilation systems: Part I–System overview and formulation. *Prog.*
609 *Oceanogr. 91*, 34-49 (2011).
610 59. Moore, A. M. et al. The Regional Ocean Modeling System (ROMS) 4-dimensional
611 variational data assimilation systems: part II–performance and application to the California
612 Current System, *Prog. Oceanogr.* ***91***, 50-73 (2011).
613 60. Broquet, G., Moore, A. M., Arango, H. G. & Edwards, C. A. Corrections to ocean surface
614 forcing in the California Current System using 4D variational data assimilation. *Ocean*
615 *Modell.* **36**, 116-132 (2011).
616 61. Kara, A. B., Rochford, P. A. & Hurlburt, H. E. An optimal definition for ocean mixed layer
617 depth. *J. Geophys. Res.* **105**, 16803-16821 (2000).
618 62. Palacios, D. M., Hazen, E. L., Schroeder, I. D. & Bograd, S. J. Modeling the temperature-
619 nitrate relationship in the coastal upwelling domain of the California Current. *J. Geophys.*
620 *Res*. **118**, 3223–3239 (2013).
621 63. Largier, J. L., Magnell, B. A. & Winant, C. D. Subtidal circulation over the northern
622 California shelf. *J. Geophys. Res.* **98**, 18147-18179 (1993).
623 64. Wilkerson, F. P., Lassiter, A. M., Dugdale, R. C., Marchi, A. & Hogue, V. E. The
624 phytoplankton bloom response to wind events and upwelled nutrients during the CoOP
625 WEST study. *Deep Sea Res. Part II* **53**, 3023-3048 (2006).
626 65. Bograd, S. J. et al. Phenology of coastal upwelling in the California Current. *Geophys. Res.*
627 *Lett.* **36** (2009).
628

Acknowledgments

We thank the ocean modeling group at UCSC for providing the model output used for analysis herein (available from http://oceanmodeling.ucsc.edu). We are also grateful to Cisco Werner, Toby Garfield, and three anonymous reviewers for comments on an earlier version of the manuscript. This research was supported by NOAA's California Current Integrated Ecosystem Assessment program and NSF grant OCE-1434732.

Author Contributions

M.G.J. designed the study, performed the analysis, and wrote the manuscript. S.J.B. and E.L.H. helped design the analysis. All authors discussed the results and edited the manuscript.

Author Information

The authors declare no competing financial interests.

Correspondence and requests for materials should be addressed to M.G.J. (mjacox@ucsc.edu)

643 Figures

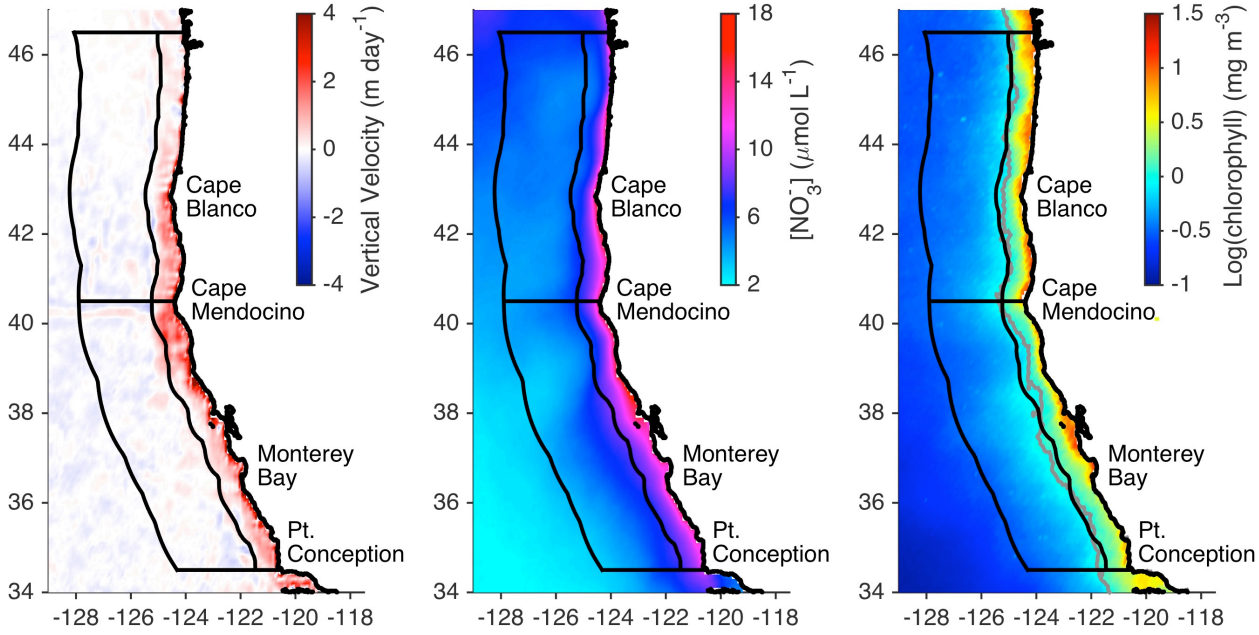

644

645 **Figure 1: Study region.** 1998-2010 March-August means of (left) model vertical velocity at the
646 base of the mixed layer, (middle) nitrate concentration at the base of the mixed layer, estimated
647 from model hydrography and observed temperature-salinity-nitrate relationships (Fig. S4), and
648 (right) SeaWiFS surface chlorophyll concentration. Details of variable calculations are provided
649 in the Methods. Black contours divide the CCS domain into northern (40.5-46.5˚N) and central
650 (34.5-40.5˚N) as well as nearshore (0-75 km from shore) and offshore (75-300 km from shore)
651 regions. The gray contour indicates surface chlorophyll concentration of 1 mg m^{-3}. Figure
652 created using MATLAB® R2015a (www.mathworks.com).

653

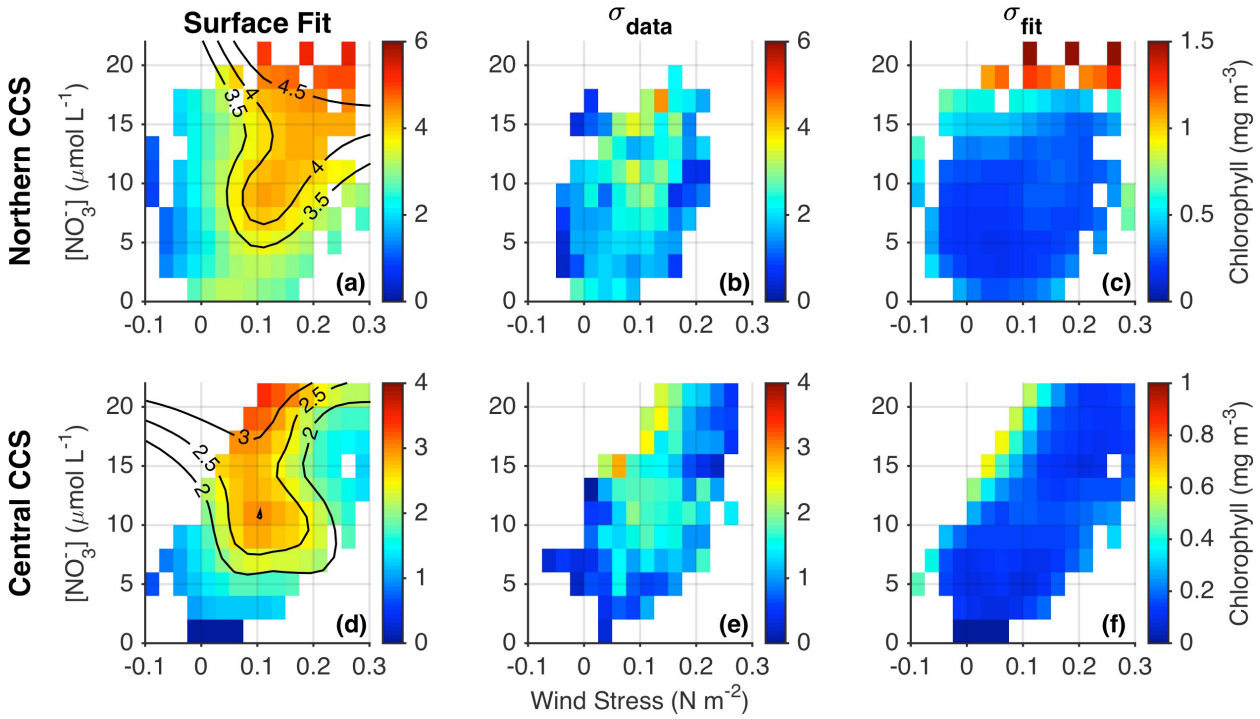

Figure 2: Chlorophyll dependence on wind stress and nitrate in the nearshore region. (a,d) Surface chlorophyll concentration, averaged from the coast to 75 km offshore, is shown as a function of alongshore wind stress (equatorward is positive) and nitrate concentration at the base of the mixed layer in the northern and central CCS regions. Alongshore wind stress is measured 75 km offshore and nitrate concentration at the base of the mixed layer is averaged over the 75 km coastal band (see Fig. 1). All variables are 8-day averages with a subsequent three-point moving average applied, increasing the effective temporal averaging to 24 days. (b,e) Standard deviations of data points within each pixel indicate spread in the data. (c,f) Standard deviation of 1000 surface fits, each performed with 50% of the data randomly withheld, indicates uncertainty in the surface fits. For (c) and (e), white pixels have fewer than 3 data points; for other panels white pixels indicate no data. Note smaller [chl] ranges in rightmost panels.

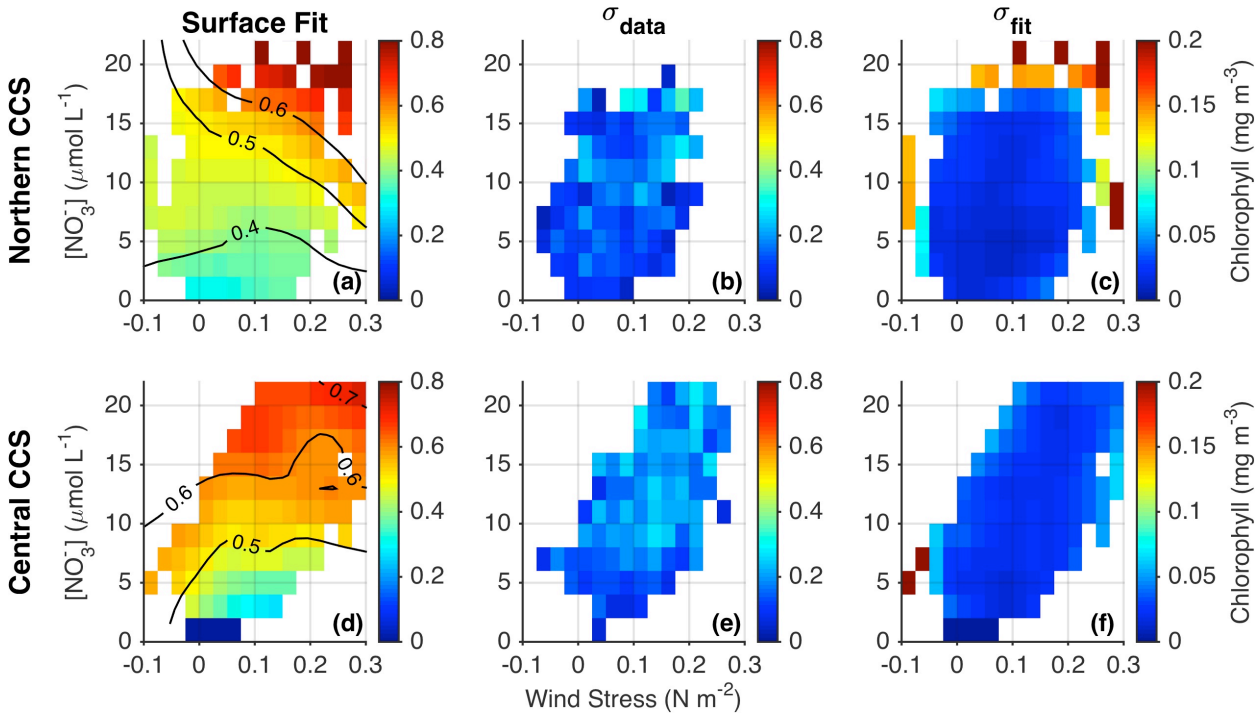

667

668 **Figure 3: Chlorophyll dependence on wind stress and nitrate in the offshore region.** As in

669 Fig. 2, but for chlorophyll averaged over the offshore region (75-300 km from shore).

670

671

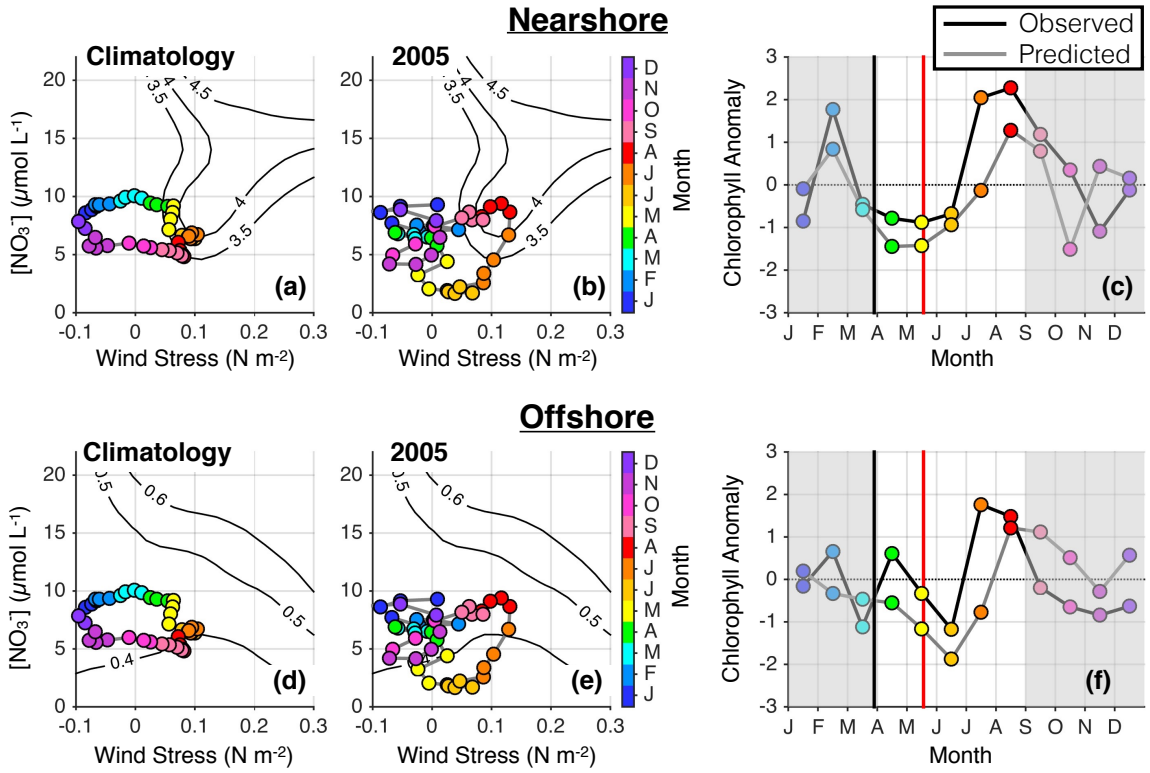

Figure 4: Delayed 2005 spring transition in the northern CCS. (a,d) Climatological and (b,e) 2005 annual progression of wind stress and nitrate concentration are shown for the (top) nearshore and (bottom) offshore regions of the northern CCS. Variables are calculated as in Fig. 2, and chlorophyll dependence on wind stress and nitrate for the nearshore (offshore) region is indicated by contours from Fig. 2a (3a). Chlorophyll anomalies are averaged over the (c) nearshore and (f) offshore regions and divided by the standard deviation of 1998-2010 monthly anomalies. Months outside of the upwelling season, which were not included when calculating the relationships in Figs. 2 and 3, are shaded in gray. Black and red vertical lines mark the climatological and 2005 Spring Transition Indices, respectively, calculated from alongshore wind as described in Bograd et al.[65].

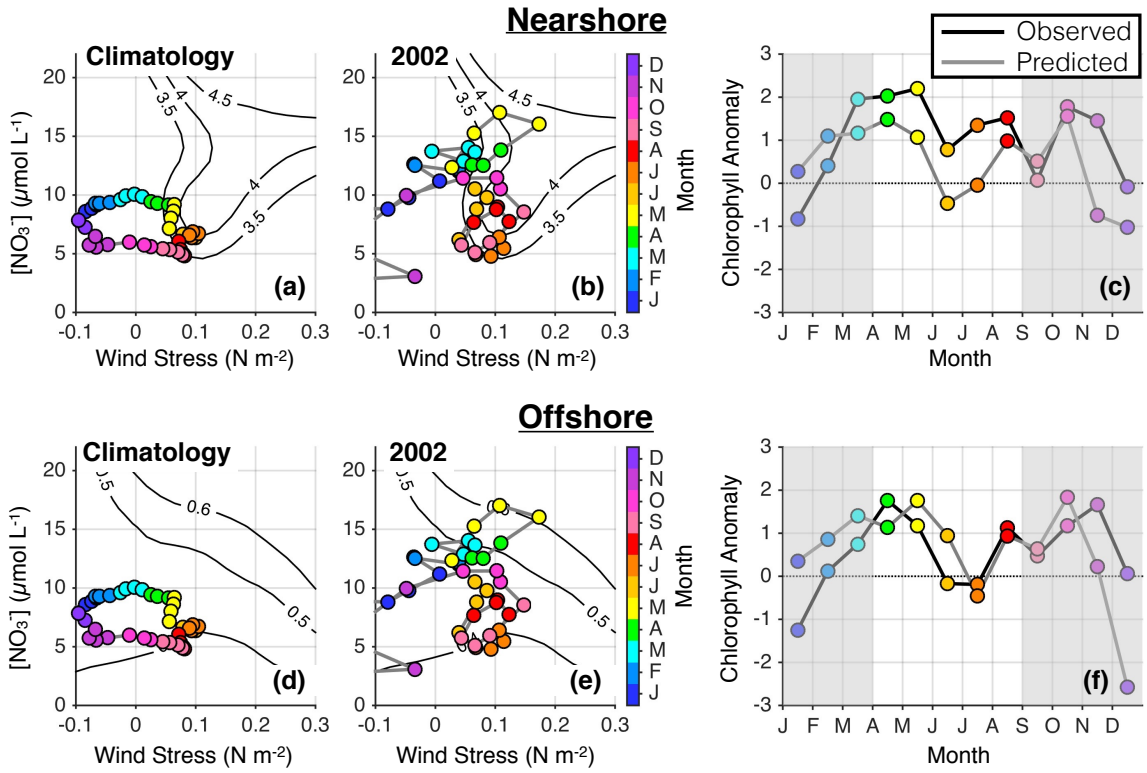

683

684 **Figure 5: Anomalous influence of nutrient-rich subarctic waters in 2002.** Line and contour

685 plots are as in Fig. 4, but for 2002.

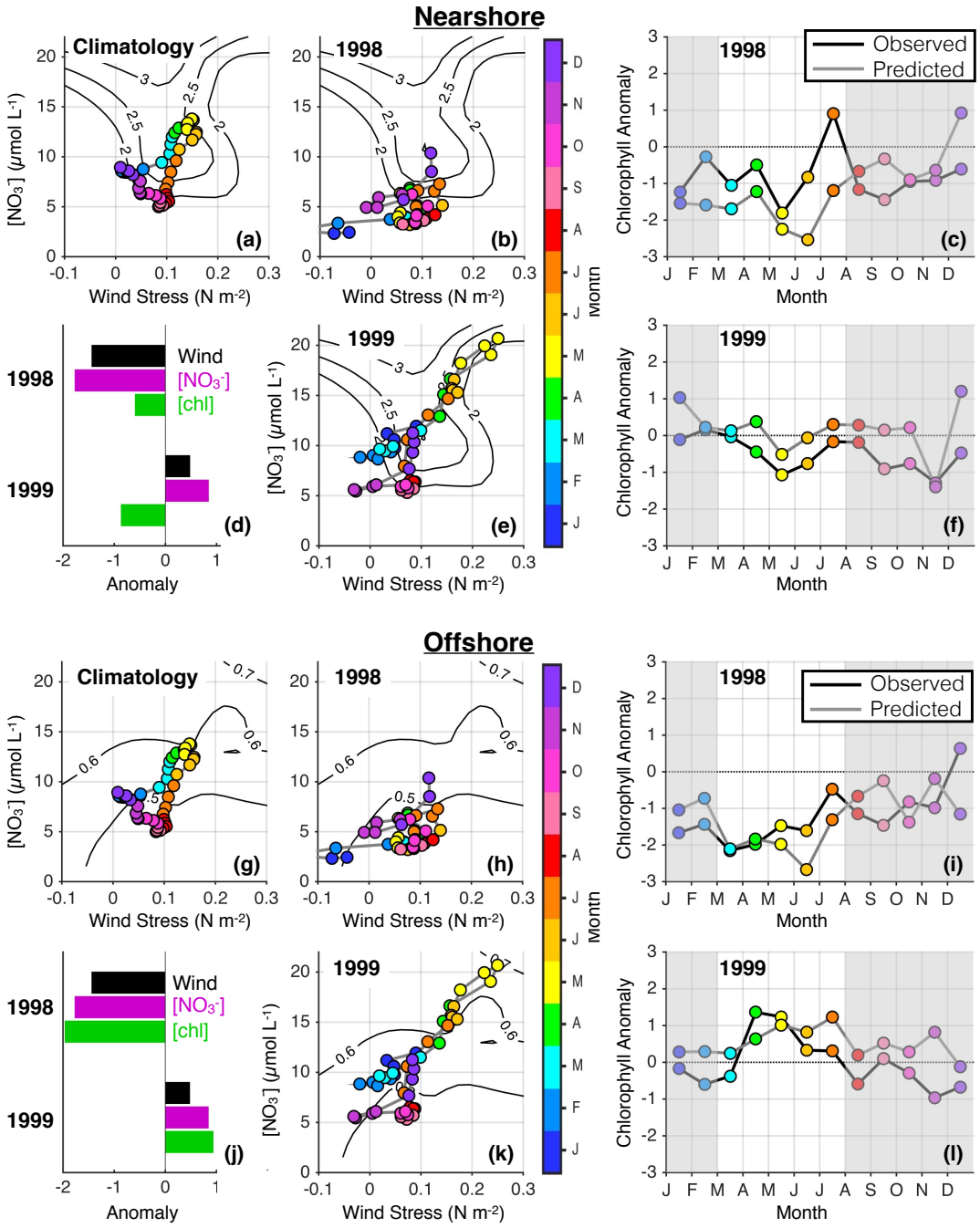

Figure 6: The 1998-1999 El Niño/La Niña cycle in the central CCS. Line and contour plots are as in Figs. 4 and 5, but for (a-f) nearshore and (g-l) offshore regions of the central CCS in 1998-1999. Chlorophyll contours are from Fig. 2d for nearshore (a,b,e) and Fig. 3d for offshore (g,h,k) plots. Bar plots (d,j) summarize March-July mean anomalies for 1998 and 1999, normalized by the standard deviation of March-July means for 1998-2010.